This work has been published in the IEEE GLOBECOM 2022 conference

Time vs. Unit Cell Splitting for Autonomous Reconfigurable Intelligent Surfaces

Konstantinos Ntontin*, Alexandros-Apostolos A. Boulogeorgos†, Zaid Abdullah*,
Agapi Mesodiakaki§,¶, Sergi Abadal‖, and Symeon Chatzinotas*

*SnT, SIGCOM, University of Luxembourg, Luxembourg,
e-mail: {kostantinos.ntontin, zaid.abdullah, symeon.chatzinotas}@uni.lu
†Department of Digital Systems, University of Piraeus, Greece, e-mail: al.boulogeorgos@ieee.org
§Department of Informatics, Aristotle University of Thessaloniki, Greece, email: amesodia@csd.auth.gr
¶Center for Interdisciplinary Research and Innovation, Thessaloniki, Greece
‖NaNoNetworking Center in Catalunya (N3Cat), Universitat Politècnica de Catalunya, Spain, email: abadal@ac.upc.edu

***Abstract*—In this work, we propose a time- and a unit cell-splitting protocol for supplying the energy needs of reconfigurable intelligent surfaces (RISs) through wireless energy harvesting (EH) from information signals. We first compute the RIS energy consumption per frame that is common for both protocols and incorporates the energy burden for channel estimation. Based on it, we subsequently formulate an optimization problem that maximizes the average rate under the constraint of meeting the RIS long-term energy consumption demands. In addition, closed-form solutions regarding the optimal allocation of resources are provided for both protocols in the case of deterministic channel gains for the transmitter-RIS links and a methodology to obtain such a solution in the general case of random channels. Finally, for the optimal resource allocation for both protocols numerical results based on Monte-Carlo simulations reveal that the unit cell-splitting protocol exhibits a superior performance compared to its time-splitting counterpart.**

***Index Terms*—Autonomous operation, reconfigurable intelligent surfaces (RISs), wireless energy harvesting (EH).**

I. Introduction

Circumventing cost and high energy consumption issues of active relays that are equipped with power-hungry amplifiers, the paradigm of reconfigurable intelligent surfaces (RISs) could potentially achieve the coverage enhancement required in dense urban scenarios, especially for millimeter wave (mmWave) bands that are highly susceptible to blockages [1]. This has led to the characterization of RISs as nearly passive structures, which raises the question of whether RISs can be powered by means of wireless energy harvesting (EH). Such a groundbreaking feature has been proposed particularly for the so-called integrated architecture for altering the impedance of the unit cells (UCs) that relies on a network of integrated and interconnected electronic chips [2].

Why autonomous RISs?: Let us first identify indicative scenarios in which autonomous RIS operation is a desirable feature. Such scenarios are depicted in Fig. 1. In particular, power-grid unavailability and aesthetics issues might limit the deployment of RISs onto objects, such as trees. In addition, due to aesthetics reasons it could be difficult to acquire permissions from the building managers to deploy exterior cables onto the facades for powering the RISs. Supplying their energy needs through batteries that are not recharged perpetually by some gridless process is also not a viable option, since they would need constant monitoring and manual replacement. Finally, in the case of RISs equipping unmanned aerial vehicles (UAVs), supplying their energy needs through the vehicle batteries remains challenging, as it would drain them faster and reduce their flight time.

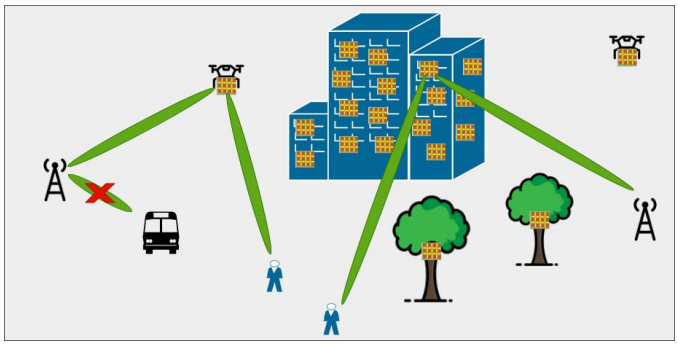

Fig. 1: Indicative scenarios in which autonomous RIS operation is desirable.

Related works: Few recent works have started incorporating the feature of autonomy by wireless EH from information signals, either through time splitting [3], [4], UC splitting [5–7], or both protocols [8]. In the time-splitting case, dedicated disjoint time intervals are allocated for either EH through absorption or information transmission through reflection. In the UC-splitting one there is a common time interval for both EH and information transmission by devoting a subset of UCs for EH and its orthogonal complement subset for information transmission. All these works consider online optimization schemes for the allocation of resources that, on the one hand, satisfy the RIS energy demands and, on the other hand, meet the end-to-end service demands.

Motivation and contribution: The aforementioned works on autonomous RISs need instantaneous channel estimates, which in several cases are very difficult or even impossible to acquire. Apart from this, the energy burden associated with

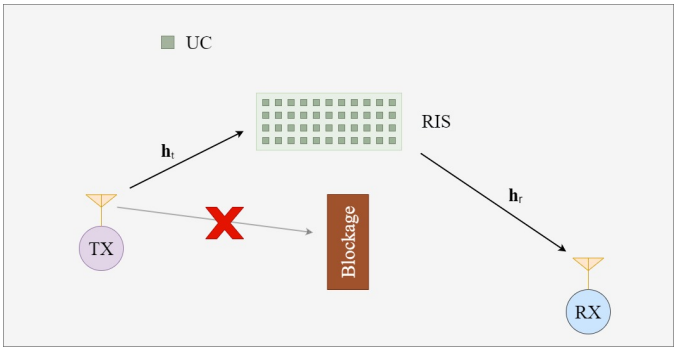

Fig. 2: RIS-assisted communication due to a blocked direct link.

the reconfigurations of the UCs needed for channel estimation is overlooked. Moreover, prior literature aims at presenting the capabilities of online learning approaches. As a consequence, they do not provide an in depth comparison of the time- and UC- splitting protocols.

Motivated by the above, the contribution of this work can be summarized as follows:

- We present a time-splitting and a UC-splitting wireless EH protocol for RISs that incorporate the channel estimation phase. This allows us to accurately compute the RIS energy consumption during a frame transmission.
- In contrast to previous works that consider online resource allocation based on instantaneous channel estimates, we consider low-complexity offline schemes for the two presented protocols, based on long-term statistics. Closed-form solutions that target the average rate maximization are provided for both protocols in the case of deterministic channel gains for the transmitter (TX)-RIS links, as well as a methodology for obtaining the solution in the general case of random channel gains.

The rest of this manuscript is structured as follows. In Section II, the system and channel models are presented together with the considered channel estimation protocol and the resulting RIS energy consumption per frame, based on the employed power-consumption model. In Section III, we initially compute the harvested energy per transmission frame. Subsequently, we introduce the proposed time- and UC-splitting protocols and, finally, we compute the instantaneous signal-to-noise ratio (SNR) and achievable rate. In Section IV, the formulation of the problem of interest is presented together with a methodology for its solution in the general case of random TX-RIS channel gains and an exact solution in the case of deterministic gains. Numerical results that substantiate the analytical findings are presented in Section V-A, while the main takeaways of this work are summarized in Section VI.

II. System, Channel, and RIS Power-Consumption Model

A. System model

As illustrated in Fig. 2, we consider a scenario in which a directional TX communicates with a directional receiver (RX) through an RIS located in the far-field of both the TX and RX. The TX-RIS link, of distance d_t m, and RIS-RX link, of distance d_r m, constitute an alternative path to the direct TX-RX link that is assumed to be blocked. The RIS is a rectangular uniform planar array consisting of $M_s = M_x \times M_y$ UCs of size $d_x \times d_y$. M_x (M_y) and d_x (d_y) denote the number of UCs and their length in the x-axis (y-axis), respectively. In addition, we assume that the RIS is not equipped with an external power supply, but it relies on EH from the incoming power related to the transmission of the TX. Through this harvested energy it can achieve autonomous operation. The transmission power of TX is equal to P_t. Finally, we assume that the received signal is subject to additive white complex Gaussian noise with power σ^2, computed in dBm as $\sigma^2 = -174 + 10\log_{10}(W) + \mathcal{F}_{\text{dB}}$, where $\mathcal{F}_{\text{dB}}$ is the noise figure of the RX in dB and W is the signal bandwidth in Hz [9].

B. Channel model

We assume a flat-fading channel model[1] where the complex envelope channel vectors of the TX-RIS and RIS-RX links can be respectively obtained as

$$\mathbf{h}_{\text{t}} = [h_{t_1} \quad \cdots \quad h_{t_{M_s}}]^T, \quad \mathbf{h}_{\text{r}} = [h_{r_1} \quad \cdots \quad h_{r_{M_s}}]^T, \quad (1)$$

where the UCs can be indexed arbitrarily. These vectors describe the joint effect of antenna gains, geometric pathloss, and multipath fading (i.e., the combination of small-scale and large-scale fading).

C. Channel-estimation protocol

For the estimation of $\mathbf{h}_{\text{t}}$ and $\mathbf{h}_{\text{r}}$, we consider the approach presented in [10] that is suitable for rank-deficient (sparse) TX-RIS and RIS-RX channels. Such a sparsity is expected to be encountered in TX-RIS and RIS-RX links that consist of few dominant components, such as the line-of-sight (LoS) component and weak diffuse ones, as it is the case with mmWave and THz channels. According to [10], for effective recovery of $\mathbf{h}_{\text{t}}$ and $\mathbf{h}_{\text{r}}$ during each time slot of the preamble duration, which we denote by N_{pr}, some of the UCs are in the 'Off' state (0 value) and some in the 'On' state (1 value) and the position of 0's and 1's changes at each slot. We denote the percentage of UCs that are in state '1' at each slot of the preamble equal to μ. As stated in [10], the recovery of the TX-RIS and RIS-RX links is more effective for low values of μ. Based on this, in the worst-case scenario the number of state changes during the training period is equal to twice the number of its 'On' states, i.e. $2\mu N_{\text{pr}}$. In addition, after the training period an additional reconfiguration of the RIS is needed where the impedance of the UCs is adjusted based on the channel estimates. Hence, the upper bound of the total

[1]The flat fading assumption can hold even in the large-bandwidth case of mmWave and THz links due to the small delay spreads associated with highly directional transmissions. Furthermore, due to the comparative nature of this work the outcomes are not expected to change in the case of frequency-selective channels.

amount of reconfigurations for the M_s UCs, which we denote by $N_{\text{rec}}^{\text{tot}}$, is given by

$$N_{\text{rec}}^{\text{tot}} = M_s \left(2\mu N_{\text{pr}} + 1\right). \tag{2}$$

D. RIS power-consumption model and total energy consumption per frame

1) RIS power-consumption modules: Under the consideration of the integrated control architecture, we assume that one chip controls the impedance of a single UC. Furthermore, for the radio frequency (RF)-to-direct currrent (DC) power conversion that is needed to power the electronic modules of the RIS, we assume that a passive rectifier circuit follows an RF combiner that combines the absorbed RF powers related to each UC [11]. Hence, the power consumption of the RIS is only the result of the static and dynamic power consumption of the M_s electronic chips that adjust the UC impedance.

2) RIS energy consumption per frame: Let us now evaluate the RIS energy consumption per frame, denoted by $E_{\text{tot}}^{\text{fr}}$. It holds that [12, Eq. (4.5)]

$$E_{\text{tot}}^{\text{fr}} = E_{\text{st}}^{\text{fr}} + E_{\text{dyn}}^{\text{fr}}, \tag{3}$$

where $E_{\text{st}}^{\text{fr}}$ and $E_{\text{dyn}}^{\text{fr}}$ denote the static and dynamic RIS energy consumption. Regarding $E_{\text{st}}^{\text{fr}}$, it is expected to scale linearly with the number of UCs. Hence, denoting the total number of time slots per frame by N_{fr}, their duration by T_{sl}, and the static power consumption per chip by P_{st}, it holds

$$E_{\text{st}}^{\text{fr}} = M_s N_{\text{fr}} T_{\text{sl}} P_{\text{st}}. \tag{4}$$

As far as $E_{\text{dyn}}^{\text{fr}}$ is concerned, based on (2) and by considering that the energy cost for a UC reconfiguration is E_{UC}, for the upper bound on $E_{\text{dyn}}^{\text{fr}}$ per frame it holds

$$E_{\text{dyn}}^{\text{fr}} = N_{\text{rec}}^{\text{tot}} E_{\text{UC}} = M_s \left(2\mu N_{\text{pr}} + 1\right) E_{\text{UC}}. \tag{5}$$

In addition, we note that in this work we consider the overprovisioning of the system in terms of EH based on the upper bound on the amount of UC reconfigurations per frame and, hence, the maximum value of $E_{\text{dyn}}^{\text{fr}}$. Consequently, based on (4) and (5), it holds

$$E_{\text{tot}}^{\text{fr}} = M_s \left(N_{\text{fr}} T_{\text{sl}} P_{\text{st}} + \left(2\mu N_{\text{pr}} + 1\right) E_{\text{UC}}\right). \tag{6}$$

III. Harvested Energy per Frame and Proposed Time/UC-Splitting Architectures

A. Harvested energy per frame

Let us denote the set of the UCs used for harvesting (the same for each frame) by $\mathcal{A}_h$ and of all the UCs by $\mathcal{A}_s$, i.e.

$$\mathcal{A}_s = \{1, 2, ..., M_s\}. \tag{7}$$

Consequently, it holds that $\mathcal{A}_h \subseteq \mathcal{A}_s$. In addition, we denote the set of the UCs dedicated for reflection by $\mathcal{A}_r$. As a result, $\mathcal{A}_r$ is the orthogonal complement of $\mathcal{A}_h$, i.e. $\mathcal{A}_r = \mathcal{A}_h^C$. Finally, the number of UCs in $\mathcal{A}_h$ and $\mathcal{A}_r$ is denoted by M_h and M_r, respectively. Hence, $M_h + M_r = M_s$.

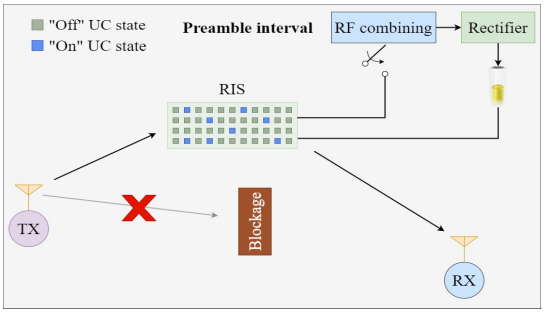

Fig. 3: Preamble phase, common for both the proposed time-splitting and UC-splitting protocols.

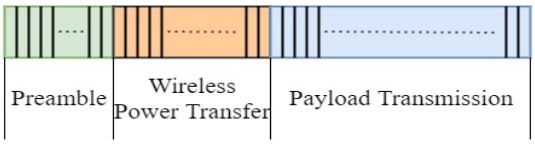

Fig. 4: Frame structure in the time-splitting protocol.

As for the DC harvested power at a time slot of the n_{th} frame dedicated for EH, either solely or in parallel with information transmission, denoted by $P_{\text{DC}}\left(\mathcal{A}_h\right)$, it holds [13]

$$P_{\text{DC}}\left(\mathcal{A}_h\right) = \frac{\frac{P_{\max}}{1+e^{-a\left(P_{\text{RF}}\left(\mathcal{A}_h\right)-b\right)}} - \frac{P_{\max}}{1+e^{ab}}}{1 - \frac{1}{1+e^{ab}}}, \tag{8}$$

where $P_{\text{RF}}\left(\mathcal{A}_h\right)$ is the harvested RF power that is inputted to the rectifier and $P_{\max}$ is a constant denoting the maximum harvested power when the harvesting circuit at the rectifier is saturated. In addition, a and b are circuit-specific parameters, which are related to the resistance, capacitance, and turn-on voltage of the diode used for rectification. The non-linear model of (8) has been extensively validated through experimental measurements [13].

Regarding $P_{\text{RF}}\left(\mathcal{A}_h\right)$, it is given by

$$P_{\text{RF}}\left(\mathcal{A}_h\right) = P_t \sum_{i \in \mathcal{A}_h} \left|h_{t_i}\right|^2, \tag{9}$$

where P_t is the TX power. Finally, by denoting the number of time slots (the same for each frame) dedicated to EH by N_h and the amount of the harvested energy by E_h, it holds

$$E_h = P_{\text{DC}}\left(\mathcal{A}_h\right) N_h T_{\text{sl}}. \tag{10}$$

B. Proposed time-splitting protocol

In the proposed time-splitting protocol, after the preamble phase that is depicted in a time interval for wireless power transfer follows where all the UCs of the RIS are dedicated to EH. This interval has a duration of N_{pt} slots. Finally, the payload transmission interval follows with a duration of N_{pl} time slots where all the UCs of the RIS are dedicated to focusing towards the RX through perfect reflection. By denoting the number of time slots in a frame as N_{fr}, it holds

$$N_{\text{fr}} = N_{\text{pr}} + N_{\text{pt}} + N_{\text{pl}}. \tag{11}$$

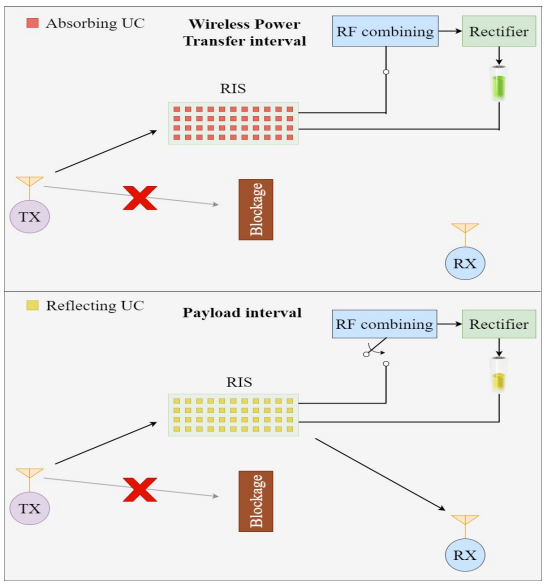

Fig. 5: Post-preamble time-splitting protocol functionality.

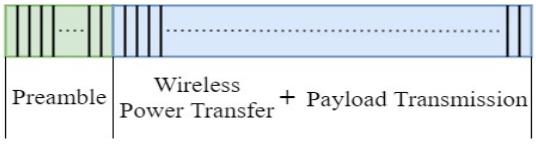

Fig. 6: Frame structure in the UC-splitting architecture.

Illustratively, the frame structure is depicted in Fig. 4 and the functionality of the RIS for the post-preamble frame intervals is depicted in Fig. 5.

C. Proposed UC-splitting protocol

The frame structure is depicted in Fig. 6. After the preamble transmission, simultaneous wireless power transfer and information transmission are realized by dedicating a subset of UCs for EH through perfect absorption and the rest for information transmission by acting as perfect reflectors and focusing towards the RX. Illustratively, the functionality of the RIS for the post-preamble frame interval is depicted in Fig. 7. In addition, in the UC-splitting protocol it holds that $N_{\rm pt}=0$. Hence,

$$N_{\rm fr}=N_{\rm pr}+N_{\rm pl}. \tag{12}$$

D. Instantaneous SNR and rate

1) SNR: After adjusting the UCs impedance so that the departing signals from the UCs are coherently combined at the RX, the maximum instantaneous SNR related to information transmission towards the RC, denoted by γ, can be obtained by following the standard approach as in [9].

$$\gamma=\frac{P_t}{\sigma^2}\left(\sum_{k\in\mathcal{A}_r}|h_{t_k}||h_{r_k}|\right)^2. \tag{13}$$

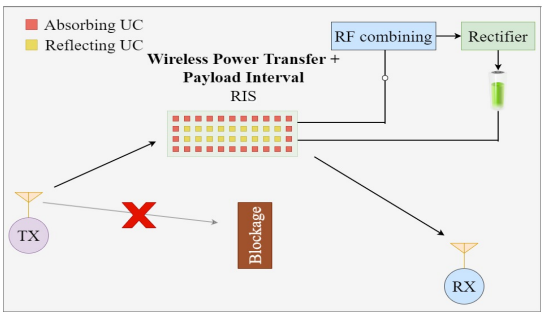

Fig. 7: Post-preamble UC-splitting protocol functionality.

2) Rate: Based on (13), the instantaneous rate R is given by

$$R=\frac{N_{\rm pl}}{N_{\rm fr}}W\log_2\left(1+\frac{P_t}{\sigma^2}\left(\sum_{k\in\mathcal{A}_r}|h_{t_k}||h_{r_k}|\right)^2\right). \tag{14}$$

IV. Problem Formulation and Solution

We target the allocation of the resources in a way that the achievable average rate in a duration of a sufficiently large number of frames, denoted by K, is maximized. At the same time, the probability that the harvested energy, denoted by $E_{1\to K}$, in the K-frame duration is smaller than the corresponding RIS energy consumption requirements should not exceed a threshold.

A. Time-splitting protocol

It holds

$$E_{1\to K}=\sum_{n=1}^{K}E_h=\left(N_{\rm fr}-N_{\rm pr}-N_{\rm pl}\right)T_{\rm sl}\sum_{n=1}^{K}P_{\rm DC}\left(\mathcal{A}_s\right). \tag{15}$$

Problem A: Average rate maximization: This problem is formulated as

$$\begin{aligned}\underset{N_{\rm pl}}{\text{maximize}}\quad & \bar{R}^{(K)}\left(N_{\rm pl}\right)\\ \text{subject to}\quad & \Pr\left\{E_{1\to K}\le KE_{\rm tot}^{\rm fr}\right\}\le\epsilon,\end{aligned} \tag{16}$$

where ϵ is an outage probability threshold, $\bar{R}^{(K)}\{\cdot\}$ denotes the average rate value for the K-frame duration, and $\Pr\{\cdot\}$ denotes probability. We note that for sufficiently large K it holds that $\bar{R}^{(K)}\left(N_{\rm pl}\right)\cong\bar{R}\left(N_{\rm pl}\right)$, where $\bar{R}\left(N_{\rm pl}\right)$ is the mean value of $R\left(N_{\rm pl}\right)$, due to the law of large numbers. Based on (14) and (15), (16) can be rewritten as

$$\begin{aligned}\underset{N_{\rm pl}}{\text{maximize}}\quad & N_{\rm pl}\\ \text{subject to}\quad & \Pr\left\{\sum_{n=1}^{K}P_{\rm DC}\left(\mathcal{A}_s\right)\le\frac{KE_{\rm tot}^{\rm fr}}{\left(N_{\rm fr}-N_{\rm pr}-N_{\rm pl}\right)T_{\rm sl}}\right\}\le\epsilon.\end{aligned} \tag{17}$$

According to (17), we understand that the computation of the optimal value of $N_{\rm pl}$, which we denote by $N_{\rm pl}^*$, requires the knowledge of the cumulative density function (CDF) of $\sum_{n=1}^{K}P_{\rm DC}\left(\mathcal{A}_h\right)$, where $\mathcal{A}_h\subseteq\mathcal{A}_s$.

B. UC-splitting protocol

It holds

$$E_{1\to K}=\sum_{n=1}^{K}E_h=(N_{\rm fr}-N_{\rm pr})\,T_{\rm sl}\sum_{n=1}^{K}P_{\rm DC}\left(\mathcal{A}_h\right). \quad (18)$$

Problem B: Average rate maximization: The problem is formulated as

$$\begin{aligned}\underset{M_r}{\text{maximize}} \quad & \bar{R}^{(K)}\left(M_r\right)\\ \text{subject to} \quad & \Pr\left\{E_{1\to K}\le KE_{\rm tot}^{\rm fr}\right\}\le\epsilon.\end{aligned} \quad (19)$$

Based on (14) and (18), (19) can be rewritten as

$$\begin{aligned}\underset{M_r}{\text{maximize}} \quad & M_r\\ \text{subject to} \quad & \Pr\left\{\sum_{n=1}^{K}P_{\rm DC}\left(\mathcal{A}_h\right)\le\frac{KE_{\rm tot}^{\rm fr}}{(N_{\rm fr}-N_{\rm pr})T_{\rm sl}}\right\}\le\epsilon.\end{aligned} \quad (20)$$

According to (20) and similar to the time-splitting case, the computation of the optimal value of M_r, which we denote by M_r^*, requires the knowledge of the CDF of $\sum_{n=1}^{K}P_{\rm DC}\left(\mathcal{A}_h\right)$.

C. Computation of the CDF of $\sum_{n=1}^{K}P_{\rm DC}\left(\mathcal{A}_h\right)$

Proposition 1: The CDF of $\sum_{n=1}^{K}P_{\rm DC}\left(\mathcal{A}_h\right)$ is uniquely determined by the knowledge of the CDF of $\sum_{i\in\mathcal{A}_h}|h_{t_i}|^2$.

Proof: By considering that the channel gains among different frames are independent, $\sum_{n=1}^{K}P_{\rm DC}\left(\mathcal{A}_h\right)$ consists of the summation of K independent random variables following the same distribution. Hence, its moment generating function (MGF) is given by the MGF of the particular distribution raised at the power of K. Regarding the MGF of the mentioned distribution, it is uniquely determined by the CDF of $P_{\rm DC}\left(\mathcal{A}_h\right)$, which we denote by $F_{\rm DC}\left(x\right)$. From (8) it holds that

$$F_{\rm DC}\left(x\right)=F_{|h_t|}\left(\frac{1}{P_t}\left(-\frac{1}{a}\ln\left(\frac{P_{\max}}{x\left(1-\frac{1}{1+e^{ab}}\right)+\frac{P_{\max}}{1+e^{ab}}}-1\right)+b\right)\right), \quad (21)$$

where $F_{|h_t|}\left(x\right)$ is the CDF of $\sum_{i\in\mathcal{A}_h}|h_{t_i}|^2$. Finally, after the computation of the MGF of $\sum_{n=1}^{K}P_{\rm DC}\left(\mathcal{A}_h\right)$ its CDF can be obtained by an inverse transform.

Special case-Deterministic TX-RIS links:

Proposition 2: In the case of deterministic TX-RIS links, such as the case of free-space propagation, for which $|h_{t_i}|=c$, N_{pl}^* and M_r^* are given by

$$N_{\rm pl}^*=\left\lfloor-\frac{1}{T_{\rm sl}}\frac{E_{\rm tot}^{\rm fr}\left(1-\frac{1}{1+e^{ab}}\right)}{\frac{P_{\max}}{1+e^{-a(P_tM_sc-b)}}-\frac{P_{\max}}{1+e^{ab}}}+N_{\rm fr}-N_{\rm pr}\right\rfloor \quad (22)$$

and

$$M_r^*=M_s-\left\lceil\left(\frac{1}{P_tc}\left(-\frac{1}{a}\ln\left(\frac{P_{\max}}{D}-1\right)+b\right)\right)\right\rceil, \quad (23)$$

where $D=\frac{E_{\rm tot}^{\rm fr}}{(N_{\rm fr}-N_{\rm pr})T_{\rm sl}}\left(1-\frac{1}{1+e^{ab}}\right)+\frac{P_{\max}}{1+e^{ab}}$.

Proof: (22) and (23) originate by solving the constraints of (17) and (20) for $|h_{t_i}|=c$.

V. Numerical Results

A. Case study: Rician fading

Let us assume that both the TX-RIS and RIS-RX links are subject to uncorrelated[2] Rician fading, with corresponding K-factors denoted by K_1 and K_2, respectively. Furthermore, we consider that each UC is an electrically-small and low-gain element with a cosine gain pattern, with respect to the azimuth angle θ, expressed as [15]

$$G_s\left(\theta\right)=4\cos\left(\theta\right),\quad 0\le\theta<\pi/2. \quad (24)$$

Finally, by G_t and G_r, we denote the gains of the TX and RX antennas in the directions of the RIS. Based on these, it holds that

$$\begin{aligned}\mathbf{h}_{\rm t}&=\sqrt{\left(\frac{\lambda}{4\pi}\right)^2\frac{G_tG_s\left(\theta_{\rm inc}\right)}{d_t^2}}\left[e^{j\frac{2\pi}{\lambda}d_{t_1}}+m_1\ \cdots\ e^{j\frac{2\pi}{\lambda}d_{t_{M_s}}}+m_{M_s}\right]\\ \mathbf{h}_{\rm r}&=\sqrt{\left(\frac{\lambda}{4\pi}\right)^2\frac{G_rG_s\left(\theta_{\rm dep}\right)}{d_r^2}}\left[e^{j\frac{2\pi}{\lambda}d_{r_1}}+p_1\ \cdots\ e^{j\frac{2\pi}{\lambda}d_{r_{M_s}}}+p_{M_s}\right],\end{aligned} \quad (25)$$

where λ is the wavelength and d_{t_k}, d_{r_k}, $k=1,2,....,M_s$, are the distances between the TX and the center of the $k_{\rm th}$ UC and between the center of the $k_{\rm th}$ UC and the RX, respectively. Furthermore, $\theta_{\rm inc}$ and $\theta_{\rm dep}$ denote the incident angle on the RIS and departure angle from the RIS of the dominant LoS component, respectively. In addition, $m_k\in\mathcal{CN}\left(0,\sigma_t^2\right)$ and $p_k\in\mathcal{CN}\left(0,\sigma_r^2\right)$ represent the multipath complex envelopes of the Rayleigh fading describing the diffuse scattering in the TX-RIS and RIS-RX links, respectively.

B. Results

TABLE I: Parameter values used in the simulation.

Parameter	Value	Parameter	Value
f	28 GHz	d_x, d_y	$\lambda/2$
M_x, M_y	15	σ_t^2	0
P_t	1 W	σ_r^2	0.3
G_t	40 dBi	G_r	22 dBi
d_t	19 m	d_r	38 m
$N_{\rm fr}$	10^4	$N_{\rm pr}$	10^3
$\theta_{\rm inc}$	45°	$\theta_{\rm dep}$	60°
$\mathcal{F}_{\rm dB}$	10 dB	a	120
b	10^{-3}	$P_{\max}$	20 mW
W	100 MHz	$\eta_{\rm RF}$	0.5
$P_{\rm st}$	2 μW	$T_{\rm sl}$	1 μs
μ	0.2	K	10^4

We consider the parameter values of Table I. Since free-space propagation is assumed for the TX-RIS links ($\sigma_t^2=0$), $N_{\rm pl}^*$ and M_r^* for the time- and UC-splitting protocols are given by (22) and (23), respectively. Fig. 8 depicts the average rate in both cases versus $E_{\rm UC}$. As we observe, the UC-splitting protocol substantially outperforms its time-splitting counterpart. This is further substantiated by Fig. 9 that illustrates

[2]This approximately holds only for d_x and d_y equal to half wavelength [14]. However, any correlation among the links can be readily incorporated into the framework according to the model of [14].

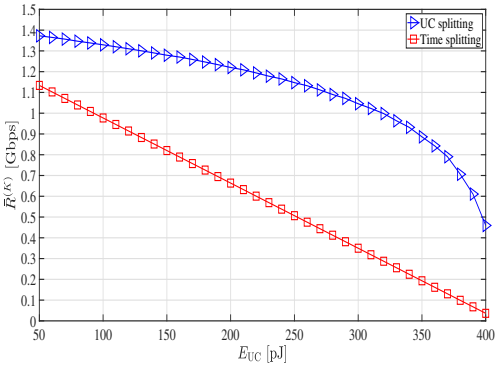

Fig. 8: K-frame average rate vs. the energy cost of a UC reconfiguration.

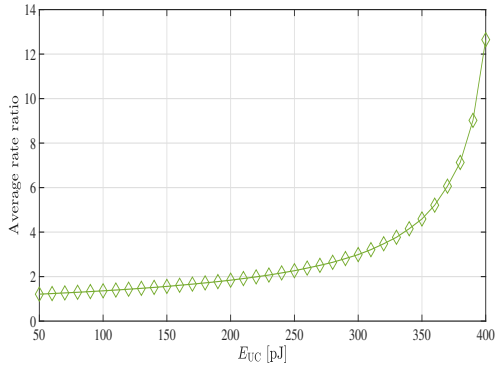

Fig. 9: Average rate ratio vs. E_{UC}.

the ratio of the average rate of the UC-splitting protocol over the corresponding one of the time-splitting protocol. As we observe, the gap increases for increasing E_{UC}. This is attributed to the fact that the corresponding reduction of the the resources allocated to reflection affects the multiplicative term outside the logarithm function in the time-splitting protocol, whereas it affects the SNR term inside the logarithm function in the UC-splitting protocol, according to (14). Consequently, the effect on the time-splitting protocol is more pronounced.

VI. Conclusions

We have conducted this work to give an answer to system designers of whether a time-splitting or a UC-splitting protocol for autonomous RIS operation is more beneficial in terms of average rate. Towards the aforementioned goal, we have proposed two realistic protocols for such architectures that take into account the energy consumption demands for channel estimation. In addition, for both architectures we have considered low-complexity offline schemes for the optimal allocation of resources for EH, based on long-term statistics that involve the average rate maximization while meeting the long-term RIS energy consumption demands. A closed-form solution was provided in the case of deterministic channel gains for the TX-RIS links and a methodology to obtain such solution in the case of random channels. Numerical results reveal that the UC-splitting protocol notably outperforms its time-splitting counterpart and the gap increases for increasing RIS energy consumption.

Acknowledgements

This work was supported by the Luxembourg National Research Fund (FNR) under the CORE project RISOTTI (ref. 14773976).

References

[1] M. Di Renzo *et al.*, "Smart Radio Environments Empowered by Reconfigurable Intelligent Surfaces: How It Works, State of Research, and The Road Ahead," *IEEE J. Sel. Areas Commun.*, vol. 38, no. 11, pp. 2450–2525, Nov. 2020.

[2] S. Abadal, T. Cui, T. Low, and J. Georgiou, "Programmable Metamaterials for Software-Defined Electromagnetic Control: Circuits, Systems, and Architectures," *IEEE J. Emerg. Sel. Topics Power Electron.*, vol. 10, no. 1, pp. 6–19, March 2020.

[3] Y. Zou, S. Gong, J. Xu, W. Cheng, D. T. Hoang, and D. Niyato, "Wireless Powered Intelligent Reflecting Surfaces for Enhancing Wireless Communications," *IEEE Trans. Veh. Techn.*, vol. 69, no. 10, pp. 12 369–12 373, Oct. 2020.

[4] Z. Chu, P. Xiao, D. Mi, W. Hao, M. Khalily, and L.-L. Yang, "A Novel Transmission Policy for Intelligent Reflecting Surface Assisted Wireless Powered Sensor Networks," *IEEE Journal of Selected Topics in Signal Processing*, vol. 15, no. 5, pp. 1143–1158, Aug. 2021.

[5] S. Hu, Z. Wei, Y. Cai, C. Liu, D. W. K. Ng, and J. Yuan, "Robust and secure sum-rate maximization for multiuser miso downlink systems with self-sustainable irs," *IEEE Trans. Commun.*, vol. 69, no. 10, pp. 7032–7049, Oct. 2021.

[6] Y. Pan, K. Wang, C. Pan, H. Zhu, and J. Wang, "Self-Sustainable Reconfigurable Intelligent Surface Aided Simultaneous Terahertz Information and Power Transfer (STIPT)." [Online]. Available: https://arxiv.org/abs/2102.04053

[7] K. Ntontin, A. A.-A. Boulogeorgos, E. Björnson, D. Selimis, W. A. Martins, S. Abadal, A. Alexiou, F. Lazarakis, S. Kisseleff, , and S. Chatzinotas, "Autonomous reconfigurable intelligent surfaces through wireless energy harvesting," in *IEEE 95th VTC Spring*, June 2022.

[8] B. Lyu, P. Ramezani, D. T. Hoang, S. Gong, Z. Yang, and A. Jamalipour, "Optimized Energy and Information Relaying in Self-Sustainable IRS-Empowered WPCN," *IEEE Trans. Commun.*, vol. 69, no. 1, pp. 619–633, Jan. 2021.

[9] K. Ntontin, A.-A. A. Boulogeorgos, D. G. Selimis, F. I. Lazarakis, A. Alexiou, and S. Chatzinotas, "Reconfigurable Intelligent Surface Optimal Placement in Millimeter-Wave Networks," *IEEE Open J. Commun. Soc.*, vol. 2, pp. 704–718, March 2021.

[10] Z.-Q. He and X. Yuan, "Cascaded Channel Estimation for Large Intelligent Metasurface Assisted Massive MIMO," *IEEE Wirel. Commun. Lett.*, vol. 9, no. 2, Feb. 2020.

[11] D. Altinel and G. K. Kurt, "Diversity Combining for RF Energy Harvesting," in *IEEE 85th VTC Spring*, 2017.

[12] "Report on the comparison between ideal HyperSurface (HSF)s and the manufactured prototypes," VISORSURF project, Tech. Rep., Dec. 2020. [Online]. Available: https://ec.europa.eu/research/participants/documents/downloadPublic?documentIds=080166e5d7993c7d&appId=PPGMS

[13] E. Boshkovska, D. W. K. Ng, N. Zlatanov, and R. Schober, "Practical Non-Linear Energy Harvesting Model and Resource Allocation for SWIPT Systems," *IEEE Commun. Lett.*, vol. 19, no. 12, pp. 2082–2085, Dec. 2015.

[14] E. Björnson and L. Sanguinetti, "Rayleigh Fading Modeling and Channel Hardening for Reconfigurable Intelligent Surfaces," *IEEE Wireless Commun.Lett.*, vol. 10, no. 4, pp. 830–834, April 2021.

[15] W. Tang, X. Chen, M. Z. Chen, J. Y. Dai, Y. Han, M. D. Renzo, S. Jin, Q. Cheng, and T. J. Cui, "Path Loss Modeling and Measurements for Reconfigurable Intelligent Surfaces in the Millimeter-Wave Frequency Band," *arXiv:1906.09490*.